The Synthesis of SERS-Active Gold Nanoflower Tags for *In Vivo* Applications

Jianping Xie,[†] Qingbo Zhang,[‡] Jim Yang Lee,[†,‡,*] and Daniel I. C. Wang[†,§]

[†]Singapore—MIT Alliance, 4 Engineering Drive 3, National University of Singapore, Singapore 117576, [‡]Department of Chemical and Biomolecular Engineering, National University of Singapore, 10 Kent Ridge Crescent, Singapore 119260, and [§]Department of Chemical Engineering, Massachusetts Institute of Technology, 77 Massachusetts Avenue, Cambridge, Massachusetts 02139

ABSTRACT This paper reports a simple, one-pot, template-free synthesis of flower-like Au nanoparticles (three-dimensional branched nanoparticles with more than 10 tips) with high yield and good size monodispersity at room temperature. The size of the Au nanoflowers could be tuned by controlling the composition of the starting reaction mixture. The key synthesis strategy was to use a common Good's buffer, HEPES, as a weak reducing and particle stabilizing agent to confine the growth of the Au nanocrystals in the special reaction region of limited ligand protection (LLP). Time-course measurements by UV—vis spectroscopy and TEM were used to follow the reaction progress and the evolution of the flower-like shape. The Au nanoflowers exhibited strong surface-enhanced effects which were utilized in the design of an efficient, stable, and nontoxic Raman-active tag for *in vivo* applications.

KEYWORDS: gold · nanoflowers · SERS · limited ligand protection · Raman tags · living cells

The use of Au nanoparticles as an optical label, a near-field optical probe, and an active substrate for surface-enhanced Raman scattering (SERS) leverages heavily upon their size and shape-dependent surface plasmon resonance (SPR) properties.[1−4] There is, therefore, strong interest in the synthesis of nanogold in various controlled shapes. While there are good recipes for the synthesis of zero-dimensional (0D, *e.g.*, spheres[4] and cubes[5]), one-dimensional (1D, *e.g.*, rods[6,7]), and two-dimensional (2D, *e.g.*, plates[8,9]) Au nanostructures, the same cannot be said about the synthesis of nanogold with complex three-dimensional structures (3D, *e.g.*, dendrites, multipods, and highly branched hyperpods such as nanoflowers (NFs)). On the other hand, since experimental measurements[10] and theoretical calculations[11−13] have shown strong enhancement of the electromagnetic field near the surface of these complex Au nanostructures, their synthesis is of interest to SERS spectroscopy and some other related optical applications.

The synthesis of branched and flower-shaped nanometals is a fairly recent development.[11−19] There are three principal strategies for generating these complex nanostructures. Template-based synthesis is the first approach. For example, liposome may be used as the soft template to guide the formation of dendritic Pt sheets.[14,15] The second approach is based on the phenomenon of oriented attachment of primary nanoparticles when surfaces with similar atomic arrangements approach each other. The synthesis of dendritic PtRu nanoparticles from faceted PtRu primary nanoparticles was based on this principle.[16] The third approach relies on the use of specific capping agents to induce anisotropic growth. The syntheses of Pt[17] and Au[11,18,19] multipods in the presence of poly(vinylpyrrolidone) (PVP) or cetyltrimethylammonium bromide (CTAB) are examples. Recently, we have also reported a "green chemistry" approach where a common Good's buffer, 2-[4-(2-hydroxyethyl)-1-piperazinyl]ethanesulfonic acid (HEPES), was used as the reducing *cum* shape-directing agent to form Au multipods with one to eight tips.[20] Thus far, these methods are able to produce Au multipods with a limited number of tips (less than 10);[11,18−20] the formation of highly branched (>10 tips) complex 3D (flower-like) nanoparticles[12,13,21,22] and the control of the size of these particles remain as a challenge.

Recently, Peng and co-workers[23,24] reported the synthesis of nanoflowers of a few metal oxides by coupling 3D oriented attachment with particle growth in the special reaction region of limited ligand protection (LLP). Compared to the sufficient ligand protection (SLP) reaction region, the LLP domain could not provide enough protection

*Address correspondence to cheleejy@nus.edu.sg.

Received for review July 13, 2008 and accepted November 13, 2008.

Published online November 25, 2008.
10.1021/nn800442q CCC: $40.75

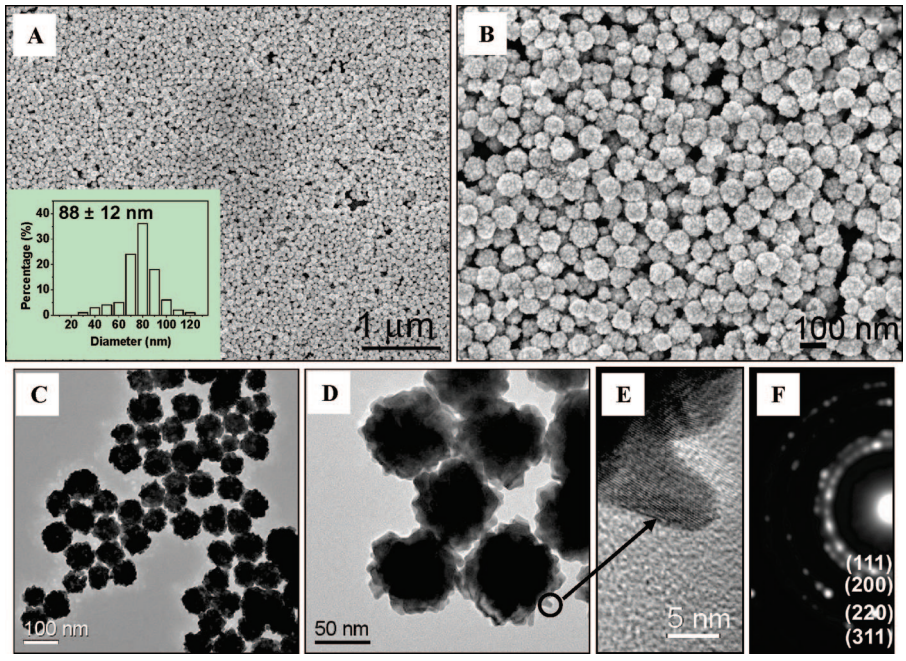

Figure 1. Representative FESEM (A and B) and TEM (C-E) images of Au nanoflowers synthesized by the reduction of $AuCl_4^-$ ions (0.5 mM) in HEPES solution (10 mM). The inset in (A) shows the histogram of distribution of sizes of Au nanoflowers. (F) The SAED pattern of the Au nanoflowers. The diffraction ring pattern is characteristic of polycrystalline Au.

for the crystal growth by the ligands, which could induce crystal aggregation or oriented attachment. Herein, we present a modified HEPES reduction method to produce metallic (Au) nanocrystals with flower-like structures in high yield and good size monodispersity. We will show that, by confining the growth of Au nanocrystals in the LLP domain, the primary nanocrystals could agglomerate to form intermediate particles which can then grow anisotropically into crystalline Au nanoflowers with 10 or more tips per particle. The size of the nanoflowers could be tuned by controlling the reaction conditions at room temperature. The HEPES coating on the Au nanoflowers imparts good biocompatibility and considerable environmental and cost advantages. The coating also provides a relatively "clean" surface where postsynthesis surface modifications may be carried out easily for biological applications. The as-synthesized Au nanoflowers are ideal SERS substrates because of the abundance of "hot" spots generated by their special surface topography which could result in substantial local electromagnetic field enhancement.[10−13] We will demonstrate this by using Au nanoflowers as a stable SERS-active tag for living cells. Presented below are the details of this investigation.

RESULTS AND DISCUSSION

Size-Controlled Synthesis of Au Nanoflowers. The current method of preparation is an extension of our previous discovery[20] that HEPES could be used as a reducing *cum* capping agent in Au nanoparticle synthesis. HEPES, a common Good's buffer in chemistry and biochemistry laboratories,[25,26] is a weak reducing agent for the Au ions ($AuCl_4^-$)[20,27] and a weak capping agent for the Au nanocrystals formed. The Au nanoflowers in this work were synthesized by confining the crystal growth in the LLP region. In a typical experiment, 0.25 mL of 20 mM $HAuCl_4$ was added to 10 mL of HEPES solution (pH 7.4) of a known initial condition (10, 15, 20, or 40 mM; corresponding to HEPES to $HAuCl_4$ mole ratios ($R_{[HEPES]/[Au]}$) of 20, 30, 40, and 80, respectively). The initially light yellow mixture changed to a color ranging from blue ([HEPES] = 10 mM) to purple ([HEPES] = 40 mM) in 30 min. The product nanoparticles were recovered by low speed centrifugation (3000 rpm for 10 min).

Figure 1A−D shows typical FESEM and TEM images of the Au nanoflowers synthesized in 10 mM HEPES solution. The as-synthesized nanocrystals were quasi-spherical, consisting of a solid core with many (>10) short, irregular, and obtuse branches. The average overall dimension of these quasi-spherical nanoflowers was 88 ± 12 nm (see inset in Figure 1A for the histogram of size distribution), and the branches had a variety of shapes and sizes. The TEM image (Figure 1C,D) of individual nanocrystals exhibits regions of varying contrast starkly different from the uniformly dark particles of spherical Au nanocrystals of the same overall size.[28] The high-resolution image (Figure 1E) shows the branches as single-crystalline protrusions from the core of the nanoflower. Selected area electron diffraction (SAED, Figure 1F) shows that the nanoflowers were crystalline and randomly oriented. In addition, the electron diffraction pattern could be indexed by the face-centered cubic (fcc) structure of Au. When an extraneous protecting agent (*e.g.*, PVP) was added to the reaction mixture in a control experiment, only spherical nanoparticles (see Figure S1 in the Supporting Information for the TEM image) were formed. This indicates that LLP is a necessary condition for the growth of flower-like nanocrystals.

When the concentration of HEPES was increased to 15 and 20 mM, smaller nanoflowers with overall diameters of 65 ± 8 (Figure 2A,B) and 48 ± 6 nm (Figure 2C,D) were formed, respectively. Further increase in the HEPES concentration to 40 mM produced nanoparticles with spherical and irregular shapes approximately 5−35 nm in size (Figure 2E,F). These observations indicate that, at the fixed Au precursor concentration of 0.5 mM, a relatively high HEPES concentration (40 mM, $R_{[HEPES]/[Au]} = 80$) was required for the weakly stabilizing HEPES ligands to operate in the SLP region. HEPES

concentrations lower than 40 mM (between 10 to 20 mM; $R_{[HEPES]/[Au]}$ from 20 to 40), on the other hand, would place the nanoparticles in the LLP region where unstable nanocrystals agglomerated and grew into 3D nanoflowers.

Optical Properties of Au Nanoflowers. The formation of flower-like Au nanocrystals was also corroborated by UV−vis spectroscopy (Figure 3). The SPR of nanoflowers ~88 nm in diameter was located at 626 nm (spectrum 1). For smaller nanoflowers, the SPR shifted progressively to shorter wavelengths (to 582 nm for the 65 nm particles (spectrum 2) and to 569 nm for the 48 nm particles (spectrum 3)). The SPR of the irregular Au nanoparticles formed in the SLP region, on the other hand, was located at 548 nm (spectrum 4). Relative to Au nanospheres of the same size, the SPR of nanoflowers was substantially red-shifted. For example, nearly spherical Au particles with an average diameter of ~66 nm would absorb at ~540 nm,[28] whereas the peak of SPR absorption of 65 nm nanoflowers was located at 582 nm. This can be understood qualitatively in the framework of plasmon hybridization theory.[11−13,29] Morphologically, nanoflowers may be regarded as hybrids of spheres and branched particles. According to the theoretical calculations of Hao *et al.*,[11] Au tripods with a tip length of 27 nm have plasmon resonance at ~700 nm. The hybridization of ~540 nm for spheres (~66 nm) and ~700 nm for branched particles should result in SPR between these limits, and the experimental value of ~582 nm for the nanoflowers fell within this range.

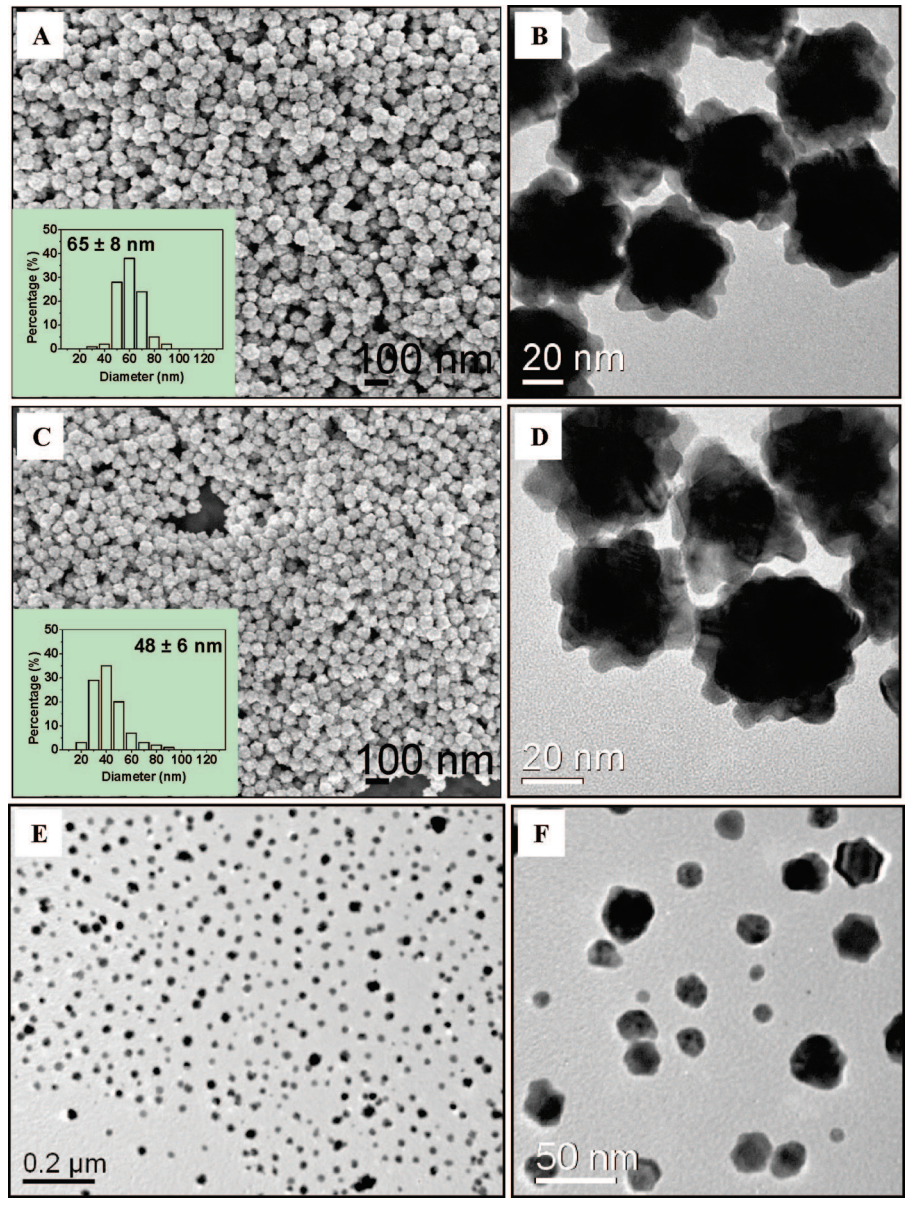

Figure 2. Representative FESEM and TEM images of Au nanocrystals formed by reducing aqueous $AuCl_4^-$ solution (0.5 mM) with HEPES solutions of different concentrations: (A and B) 15 mM, (C and D) 20 mM, and (E and F) 40 mM. The insets in (A) and (C) show the histogram of distribution of sizes of as-synthesized Au nanoflowers.

Development of Flower-like Nanostructures. The progress of reaction and the evolution of Au nanoflowers (~88 nm) as the final product were followed by time-course measurements of the UV−vis spectra (Figure 4A) and TEM images (Figure 4B). A hypothesized growth process reconstructed from these measurements is presented in Figure 4C. This particular scheme identifies three distinguishable stages: reduction of Au(III) ions to primary Au nanocrystals (stage 1), agglomeration of the primary Au nanocrystals into intermediate agglomerates (stage 2), and the anisotropic growth of the agglomerates into flower-like nanostructures (stage 3).

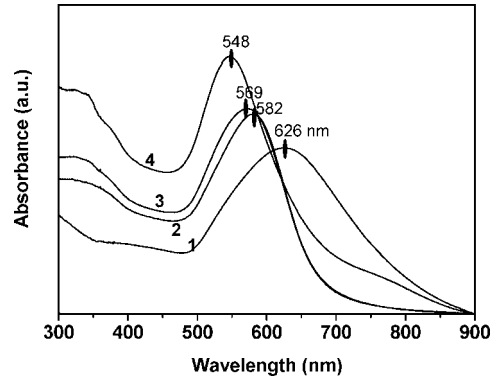

Figure 3. UV−vis spectra of Au nanocrystals formed by reducing 0.5 mM aqueous $AuCl_4^-$ solution with HEPES solutions of different concentrations. Spectra 1−4 correspond to HEPES solutions of 10, 15, 20, and 40 mM, respectively.

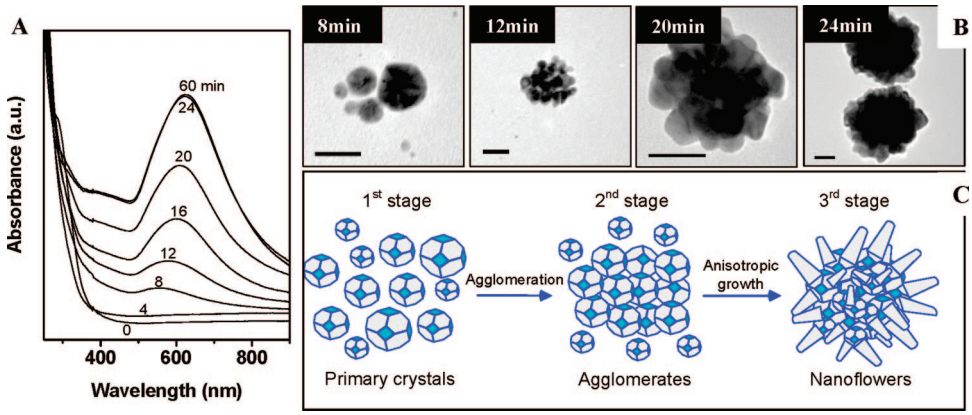

Figure 4. (A) UV−vis spectra as a function of time of reaction between aqueous $AuCl_4^-$ solution (0.5 mM) and HEPES (10 mM). (B) Representative TEM images of the products harvested at 8, 12, 20, and 24 min into the reaction. All scale bars are 20 nm. (C) Schematic illustration of the proposed mechanism for Au nanoflower formation in HEPES solution.

The color of the reaction mixture changed slowly from light yellow (0 min) to colorless (4 min), pink (8 min), purple (12 min), blue (20 min), and turbid blue finally (24 min). The pink solution after 8 min of reaction showed a weak absorption peak at 550 nm (Figure 4A), which could be attributed to the incipient formation of Au nanoparticles. The solid product recovered at 8 min was found to consist of primary Au nanocrystals 2−20 nm in size (Figure 4B). This reaction period corresponds to stage 1 of nanoflower formation: nucleation of primary Au nanocrystals. Since 10 mM HEPES solution did not provide sufficient protection for these primary Au nanocrystals (crystal growth was in the LLP region), the unstable primary nanocrystals underwent agglomeration in order to reduce the overall surface energy, signaling the beginning of stage 2. Agglomeration continued for the next 4 min, resulting in gradual changes in the solution color from pink to purple, and the red-shifting of the SPR peak (from 550 nm at 8 min to 585 nm at 12 min, Figure 4A). The morphology analysis of the product collected at 12 min, where agglomerates consisting of tens of primary crystals proliferated in the TEM image (Figure 4B, 12 min), was strong supporting evidence.

At long reaction times, the rate of reduction decreased because of the depletion of the limiting reactant (the Au precursor salt), thereby allowing the deposition of Au to follow more energetically favorable directions, resulting in the anisotropic growth of the agglomerates. Branches would protrude from the surface of the agglomerates and extend in length, forming the observed flower-like nanostructures. This was stage 3 of the growth process. TEM provided the supporting evidence for the anisotropic growth of the agglomerates between 12 and 24 min into highly branched Au nanostructures (Figure 4B). The growth of flower-like Au nanostructures from 12 to 24 min (from diameter ~38 nm @ 12 min to ~50 nm @ 20 min and to ~88 nm @ 24 min) agrees well with the red shifting of the SPR in the visible light region (585 nm @ 12 min, 608 nm @ 20 min, and 626 nm @ 24 min). The reaction was completed in approximately 24 min, as shown by no further changes in the spectra of nanoflowers recovered after 24 min of reaction and thereafter (Figure 4A). The complete reduction of Au(III) ions was also confirmed by atomic emission spectroscopy of the Au precursor solution.

In the above hypothesis, the anisotropic growth of agglomerated Au nanocrystals occurred under the condition of low residual Au ion concentration prevailing in the reaction mixture in stage 3. Low Au precursor concentration is indeed a condition generally required for the growth of branched Au nanoparticles. To prove this, a control experiment was carried out using a very low initial Au precursor concentration (0.2 mM). We used a sufficiently high concentration of the HEPES solution (40 mM, corresponding to $R_{[HEPES]/[Au]}$ of 200) to keep the reaction in the SLP region, which would normally inhibit the agglomeration of primary nanoparticles during crystal growth (stage 2). A typical FESEM image is given in Figure 5A, which shows branched particles with 1−8 tips had been formed. Evidence for the three-dimensionality of the branched particles was provided by, for instance, TEM images of particles with 3, 5, and 7 branches (see insets of Figure 5A, where the dark spots are tips radiating either inward or outward from the planes of the figures; the number of branches was confirmed

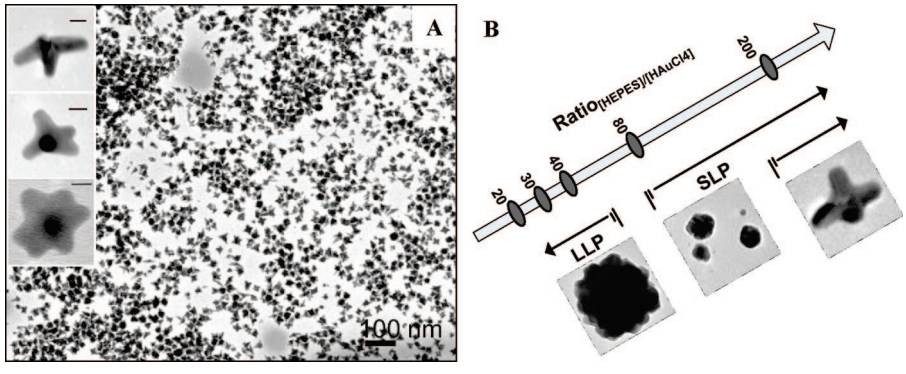

Figure 5. (A) Representative FESEM image of Au multipods synthesized by reducing 0.2 mM aqueous $AuCl_4^-$ solution with 40 mM HEPES. The insets show three multipods with 3, 5, and 7 tips, respectively. All scale bars are 20 nm. (B) Schematic illustration of the effect of $R_{[HEPES]/[Au]}$ on product morphology.

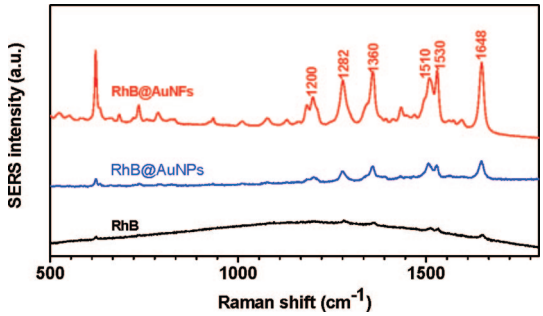

Figure 6. Typical SERS spectra of pure RhB (powder, black line), RhB on 65 nm spherical AuNPs in aqueous solution (blue line), and RhB on 88 nm AuNFs in aqueous solution (red line).

by tilting the samples). However, the number of branches that could be grown in the SLP region was limited. The development of flower-like structures with more than 10 branches was induced by applying a low Au precursor concentration in the LLP region condition (stage 3). The detailed study on the synthesis of branched Au nanocrystals with less than 10 (typically 1−8) tips has been published elsewhere.[20]

The effect of the $R_{[HEPES]/[Au]}$ ratio on product morphology is summarized in Figure 5B. Our experimental conditions spanned two distinct reaction regions (LLP and SLP). Flower-like nanoparticles were formed in the LLP region at $R_{[HEPES]/[Au]} \leq 40$, whereas single crystal nanoparticles with spherical or multipod structures were formed in the SLP region at $R_{[HEPES]/[Au]} \geq 80$.

Design and Characterizations of *d*BSA-Capped SERS Tags. Raman spectroscopy is a highly specific technique that detects and identifies molecules based on their vibrational energy levels and corresponding Raman fingerprints.[30−32] However, spontaneous Raman scattering is very weak. Colloidal Au nanoparticles have been used to increase the scattering efficiencies of Raman-active molecules by as much as $10^{14}-10^{15}$-fold.[33] Since Au nanoparticles are particularly suitable for biological applications because of their good biocompatibility and low cyctotoxicity, they may be used in the Raman spectroscopy of living cells for targeting and assaying species of interest.

Previous studies have shown that Au nanospheres (NSs) with sizes around 60−80 nm have the highest efficiency for SERS using red (633 nm) or near-infrared (785 nm) excitation.[34] Compared to these AuNSs with smooth surfaces, the as-synthesized AuNFs with an overall size of 65 or 88 nm may be a better candidate for fabricating SERS-active tags for a number of reasons: (i) tips of the nanoscale bumps or the tiny cavities on the AuNF surface are potential "hot" spots for localized near-field enhancement effects;[10−13] (ii) a larger total surface area because of the roughness of the AuNF surface; (iii) the SPR peaks of the AuNFs (*e.g.*, 626 nm for 88 nm AuNFs) are nearer to the excitation wavelength (633 nm). The closeness between the excitation and SPR wavelengths incites stronger enhancement effects.

A comparison of the Raman spectra of Rhodamine B (RhB) only (in powder form), RhB on AuNFs (using 88 nm AuNFs as an example) in aqueous solution, and RhB on AuNSs with smooth surfaces and similar particle size (~65 nm) in aqueous solution is shown in Figure 6. It is well-known that pure RhB has Raman vibrations at 1200, 1282, 1360, 1510, 1530, and 1648 cm^{-1} in the 1200−1700 cm^{-1} region.[33,35] Distinctively, Raman features were detected in RhB on AuNFs (red line) and RhB on AuNSs (blue line). The AuNFs also exhibited more than 10-fold increase in SERS intensity than the AuNSs, even though the latter were present in a concentration approximately four times that of the AuNFs.

A recent study showed that 60 nm AuNSs are much brighter (>200 times) than near-infrared-emitting quantum dots on a particle-to-particle basis.[36] In addition, nanogold has greater biocompatibility and lower cytotoxicity than quantum dots that are currently used in living cells. Thus nanogold can serve as the alternative to quantum dots for biological applications. The as-synthesized AuNFs could be turned into stable SERS-active tags with the use of a common protein, bovine serum albumin (BSA). BSA is the most abundant plasma protein and a model globular protein widely used for bionanotechnology applications.[37] It is a single polypeptide chain with a molecule weight of ~66 kDa consisting of 583 amino acid residues.[38] Figure 7A shows the design and preparation of denatured BSA (*d*BSA) protected AuNFs with embedded RhB as the Raman probe. The original AuNFs weakly protected by HEPES molecules (HEPES-capped AuNFs) were first overcoated with the Raman probe (RhB@AuNFs) and then stabilized by a layer of *d*BSA (RhB@*d*BSA-capped AuNFs) *via* the 35 thiol groups of the latter (from 35 cysteine residues[38]). The structure of AuNFs was not altered by these treatments, as confirmed by the similarity between the UV−vis spectra (Figure 7B) and FESEM images (Figure S2 in the Supporting Information) of treated and untreated Au NFs.

The intense SERS signal from RhB@*d*BSA-capped AuNFs (Figure 7C) may seem counter-intuitive given the possibility of probe molecule displacement by the thiol groups present in *d*BSA, which are strong binders for gold. The tortuous surface topology of AuNFs (*i.e.*, tips and cavities), the bulkiness of the *d*BSA molecules which increases the steric hindrance in the displacement reaction, and the delocalized π electrons in positively charged RhB which enhances the RhB binding to gold surfaces[36] are some of reasons for retaining the RhB molecules in the *d*BSA-capped tags. The preparation protocol is also applicable to other Raman probes, such as crystal violet, brilliant Green, *etc.* Compared to the original AuNFs capped by HEPES molecules, which may precipitate after long time incubation (~24 h), the as-prepared tags protected by *d*BSA have much better stability in solutions over a broad pH range (4−12), in various buffer solutions (*e.g.*, 50 mM HEPES buffer with

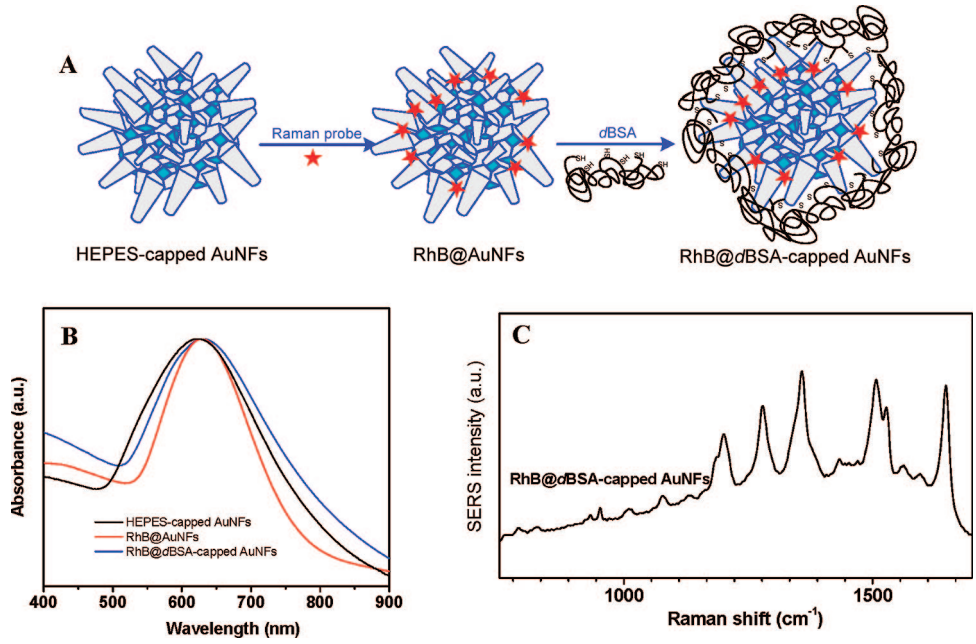

Figure 7. Design and spectroscopic properties of *d*BSA-capped SERS tags. (A) Preparation of *d*BSA-protected AuNFs as SERS tags. (B) UV−vis spectra of the HEPES-capped AuNFs (black line), RhB-capped AuNFs (blue line), and *d*BSA-capped SERS tags (red line). (C) Typical SERS spectrum of *d*BSA-capped SERS tags.

pH of 7.65), and in highly concentrated salt solutions (*e.g.*, 1 M NaCl). It is believed that the *d*BSA-protected AuNFs were stabilized by the combination of Au−S bonding with the protein (*via* the 35 Cys residues in BSA) and the bulkiness of the protein which imparts good steric protection.[39] In addition, we measured the charge of these AuNFs protected by *d*BSA at pH 7.4 and compared to the original AuNFs capped by HEPES molecules. The charge of *d*BSA-protected AuNFs is about −30 mV, which is much bigger than HEPES-capped AuNFs (~ −15 mV). This can provide additional evidence for the good stability of AuNFs protected by *d*BSA. The stability of *d*BSA-capped tags under various environmental conditions should improve their usability in both *in vitro* and *in vivo* applications. Moreover, the presence of an outer-layer of *d*BSA molecules also offers a convenient platform for further bioconjugation reactions with suitable functional ligands.

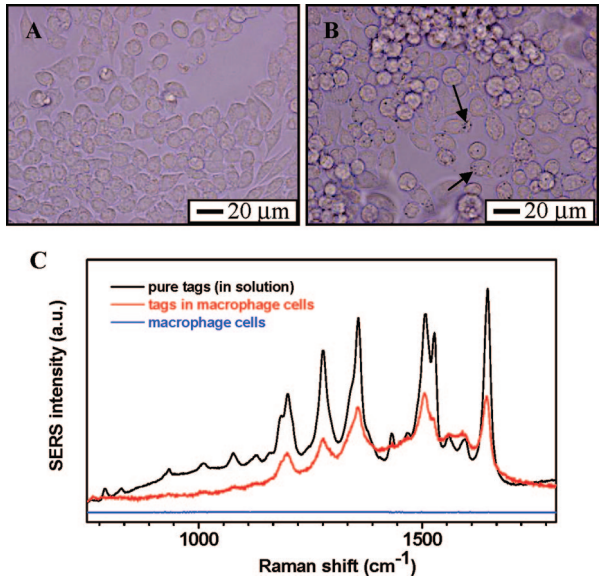

Figure 8. Live cells of a macrophage cell line (*RAW264.7*) before (A) and after uptake of *d*BSA-capped SERS tags (B). Particle accumulations are visible as black dots inside the cells (see arrows in (B)). (C) Typical SERS spectra of *d*BSA-capped SERS tags (black line), tags in living cells (red line), and living cells without tags (blue line).

We investigated the behavior of the *d*BSA-capped tags in living cells, as a proof of concept for the potential application of these tags in *in vivo* applications. The delivery of nanoparticles to the cellular interior, as well as the targeting of cellular compartments, can be achieved in various ways, depending on the cell type and the physiochemical properties of the particles.[31,40] Many cells can uptake foreign nanostructures without any induction. For example, macrophage cells can easily internalize structures smaller than 1 μm in size, with the highest efficiency shown for particles several tens of nanometers in size.[31] A common macrophage cell line, *RAW264.7* (Figure 8A), was used to explore the SERS activity of the as-prepared tags in living cells. The tags were delivered into cells grown on coverslips after 12 h of incubation, as shown in Figure 8B. At positions in the cells where the tags were present (black dots highlighted by arrows in Figure 8B), surface-enhanced Raman scattering could be detected (red line, Figure 8C), showing intensity which is characteristic of these tags in solution (black line, Figure 8C). Macrophage cells without internalization of tags showed a complete silence of the SERS signal (blue line, Figure 8C). The conservation of the SERS effects in living cells suggests that

the RhB@*d*BSA-capped AuNFs are suitable for the *in vivo* detection and targeting of tumors.

CONCLUSIONS

A simple one-pot synthesis, based on crystal growth in the LLP region, was used to produce Au nanocrystals with flower-like structures in high yield and good monodispersity. The average size of the Au nanoflowers was tunable by controlling the composition of the initial reaction mixture. The preparation could be easily scaled up to gram-quantity production. The formation of flower-like particles went through three identifiable stages: reduction of Au(III) ions to Au primary nanocrystals (stage 1), agglomeration of the primary particles to form intermediate agglomerates (stage 2), and the anisotropic growth of the agglomerates into flower-like extended structures (stage 3). The as-synthesized AuNFs exhibited strong surface-enhanced Raman scattering effects. The AuNF particles could also be developed into Raman-active tags by packaging RhB@AuNF particles with denatured BSA molecules. The application of these Raman-active tags in living cells was then demonstrated by using the *RAW264.7* macrophage cell line.

EXPERIMENTAL METHODS

Nanoparticle Synthesis. All chemicals were purchased from Sigma-Aldrich and used as received. Ultrapure Millipore water (18.2 MΩ) was used as the solvent throughout. All glassware was cleaned with Aqua Regia (HCl/HNO_3 in 3:1 ratio by volume) and rinsed with ethanol and ultrapure water *(Caution! Aqua Regia is a very corrosive oxidizing agent which should be handled with great care)*. Aqueous stock solution of HEPES with a concentration of 100 mM was prepared with ultrapure water, and its pH was adjusted to ~7.4 at 25 °C by adding 1 M NaOH solution. In a typical experiment to synthesize Au nanoflowers, 1 mL of 100 mM HEPES (pH 7.4) was mixed with 9 mL of deionized water, followed by the addition of 250 μL of 20 mM $HAuCl_4$ solution. Without shaking, the color of solution changed from light yellow to pink and finally to turbid blue at room temperature within 30 min.

Preparation of *d*BSA-Capped Raman Tags. As-synthesized Au nanoflowers (~88 nm) were recovered from a 10 mL solution by centrifugation (3000 rpm for 10 min) and rinsed three times with water. The AuNFs were then added to a 0.1 mM Rhodamine B aqueous solution. RhB-capped AuNFs were recovered 12 h later by centrifugation and dispersed in 1 mg/mL denatured BSA solution followed by 12 h of incubation. Denatured BSA was prepared by chemically treating BSA with $NaBH_4$ accordingly to a previously published procedure.[41] In brief, 165 mg of BSA was dissolved in 50 mL of deionized water, and 10 mg of $NaBH_4$ was added as a reducing agent under vigorous stirring. The reaction was allowed to proceed at room temperature for 2 h and then between 60 and 80 °C until no more gas (H_2) was liberated. BSA denatured under these conditions would have most of its disulfide bonds converted into thiol groups.

Material Characterizations. The examination of nanoparticle morphology and size was carried out on a 25 kV JEOL JSM-6700F field emission scanning electron microscope (FESEM) and on a 200kV JEOL JEM-2010 transmission electron microscope (TEM). A 200 kV JEOL JEM 2010FE was occasionally used to collect the high-resolution images. UV−vis spectroscopy made use of a Shimadzu UV-2450 spectrometer operating at 1 nm resolution. The residual Au ion concentration in the synthesis mixture was determined by atomic emission spectroscopy (AES) using a Perkin-Elmer Optima 3000DV inductively coupled plasma (ICP) spectrometer. The emission line at 242.8 nm was used to measure the concentration of elemental Au. Zeta potential measurements of AuNFs were obtained with a ZETAPALS zeta potential analyzer (Brookhaven Instruments Corporation). Raman spectra were recorded by a Renishaw inVia Raman microscope using a 633 nm laser excitation source.

Acknowledgment. J.X. acknowledges the Singapore−MIT Alliance (SMA) program for his research scholarship.

Supporting Information Available: Representative TEM images of Au nanoparticles synthesized in the presence of PVP and AuNFs protected by *d*BSA. This material is available free of charge *via* the Internet at http://pubs.acs.org.

REFERENCES AND NOTES

1. Burda, C.; Chen, X. B.; Narayanan, R.; El-Sayed, M. A. Chemistry and Properties of Nanocrystals of Different Shapes. *Chem. Rev.* **2005**, *105*, 1025–1102.
2. Eustis, S.; El-Sayed, M. A. Why Gold Nanoparticles are More Precious than Pretty Gold: Noble Metal Surface Plasmon Resonance and Its Enhancement of the Radiative and Nonradiative Properties of Nanocrystals of Different Shapes. *Chem. Soc. Rev.* **2006**, *35*, 209–217.
3. Liz-Marzan, L. M. Tailoring Surface Plasmons through the Morphology and Assembly of Metal Nanoparticles. *Langmuir* **2006**, *22*, 32–41.
4. Daniel, M. C.; Astruc, D. Gold Nanoparticles: Assembly, Supramolecular Chemistry, Quantum-Size-Related Properties, and Applications toward Biology, Catalysis, and Nanotechnology. *Chem. Rev.* **2004**, *104*, 293–346.
5. Sun, Y.; Xia, Y. Shape-Controlled Synthesis of Gold and Silver Nanoparticles. *Science* **2002**, *298*, 2176–2179.
6. Murphy, C. J.; Gole, A. M.; Hunyadi, S. E.; Orendorff, C. J. One-Dimensional Colloidal Gold and Silver Nanostructures. *Inorg. Chem.* **2006**, *45*, 7544–7554.
7. Xia, Y.; Yang, P.; Sun, Y.; Wu, Y.; Mayers, B.; Gates, B.; Yin, Y.; Kim, F.; Yan, H. One-Dimensional Nanostructures: Synthesis, Characterization, and Applications. *Adv. Mater.* **2003**, *15*, 353–389.
8. Xie, J.; Lee, J. Y.; Wang, D. I. C.; Ting, Y. P. Identification of Active Biomolecules in the High-Yield Synthesis of Single-Crystalline Gold Nanoplates in Algal Solutions. *Small* **2007**, *3*, 672–682.
9. Millstone, J. E.; Park, S.; Shuford, K. L.; Qin, L. D.; Schatz, G. C.; Mirkin, C. A. Observation of a Quadrupole Plasmon Mode for a Colloidal Solution of Gold Nanoprisms. *J. Am. Chem. Soc.* **2005**, *127*, 5312–5313.
10. Wang, H.; Halas, N. J. Mesoscopic Au "Meatball" Particles. *Adv. Mater.* **2008**, *20*, 820–825.
11. Hao, E. C.; Bailey, R. C.; Schatz, G. G.; Hupp, J. T.; Li, S. Y. Synthesis and Optical Properties of "Branched" Gold Nanocrystals. *Nano Lett.* **2004**, *4*, 327–330.
12. Bakr, O. M.; Wunsch, B. H.; Stellacci, F. High-Yield Synthesis of Multi-Branched Urchin-like Gold Nanoparticles. *Chem. Mater.* **2006**, *18*, 3297–3301.
13. Kumar, P. S.; Pastoriza-Santos, I.; Rodríguez-González, B.; García de Abajo, F. J.; Liz-Marzán, L. M. High-Yield Synthesis and Optical Response of Gold Nanostars. *Nanotechnology* **2008**, *19*, 1–5. (015606).
14. Song, Y.; Yang, Y.; Medforth, C. J.; Pereira, E.; Singh, A. K.; Xu, H.; Jiang, Y.; Brinker, C. J.; Swol, F.; Shelnutt, J. A. Controlled Synthesis of 2-D and 3-D Dendritic Platinum Nanostructures. *J. Am. Chem. Soc.* **2004**, *126*, 635–645.
15. Song, Y.; Steen, W. A.; Pena, D.; Jiang, Y. B.; Medforth, C. J.; Huo, Q.; Pincus, J. L.; Qiu, Y.; Sasaki, D. Y.; Miller, J. E.; *et al.* Foamlike Nanostructures Created from Dendritic Platinum Sheets on Liposomes. *Chem. Mater.* **2006**, *18*, 2335–2346.

16. Teng, X.; Maksimuk, S.; Frommer, S.; Yang, H. Three-Dimensional PtRu Nanostructures. *Chem. Mater.* **2007**, *19*, 36–41.
17. Chen, J.; Herricks, T.; Xia, Y. Polyol Synthesis of Platinum Nanostructures: Control of Morphology through the Manipulation of Reduction Kinetics. *Angew. Chem., Int. Ed.* **2005**, *44*, 2589–2592.
18. Chen, S. H.; Wang, Z. L.; Ballato, J.; Foulger, S. H.; Carroll, D. L. Monopod, Bipod, Tripod, and Tetrapod Gold Nanocrystals. *J. Am. Chem. Soc.* **2003**, *125*, 16186–16187.
19. Nehl, C. L.; Liao, H. W.; Hafner, J. H. Optical Properties of Star-Shaped Gold Nanoparticles. *Nano Lett.* **2006**, *6*, 683–688.
20. Xie, J.; Lee, J. Y.; Wang, D. I. C. Seedless, Surfactantless, High-Yield Synthesis of Branched Gold Nanocrystals in HEPES Buffer Solution. *Chem. Mater.* **2007**, *19*, 2823–2830.
21. Wang, W.; Cui, H. Chitosan-Luminol Reduced Gold Nanoflowers: From One-Pot Synthesis to Morphology-Dependent SPR and Chemiluminescence Sensing. *J. Phys. Chem. C* **2008**, *112*, 10759–10766.
22. Jena, B. K.; Raj, C. R. Seedless, Surfactantless Room Temperature Synthesis of Single Crystalline Fluorescent Gold Nanoflowers with Pronounced SERS and Electrocatalytic Activity. *Chem. Mater.* **2008**, *20*, 3546–3548.
23. Narayanaswamy, A.; Xu, H.; Pradhan, N.; Kim, M.; Peng, X. Formation of Nearly Monodisperse In_2O_3 Nanodots and Oriented-Attached Nanoflowers: Hydrolysis and Alcoholysis *vs* Pyrolysis. *J. Am. Chem. Soc.* **2006**, *128*, 10310–10319.
24. Narayanaswamy, A.; Xu, H.; Pradhan, N.; Peng, X. Crystalline Nanoflowers with Different Chemical Compositions and Physical Properties Grown by Limited Ligand Protection. *Angew. Chem., Int. Ed.* **2006**, *45*, 5361–5364.
25. Good, N. E.; Winget, G. D.; Winter, W.; Connolly, T. N.; Izana, K.; Singh, R. M. M. Hydrogen Ion Buffers for Biological Research. *Biochemistry* **1966**, *5*, 467–477.
26. Good, N. E.; Izawa, K. Hydrogen Ion Buffers. *Methods Enzymol.* **1972**, *24*, 53–68.
27. Habib, A.; Tabata, M.; Wu, Y. G. Formation of Gold Nanoparticles by Good's Buffers. *Bull. Chem. Soc. Jpn.* **2005**, *78*, 262–269.
28. Rodriguez-Fernandez, J.; Perez-Juste, J.; Abajo, F. J. G.; Liz-Marzan, L. M. Seeded Growth of Submicron Au Colloids with Quadrupole Plasmon Resonance Modes. *Langmuir* **2006**, *22*, 7007–7010.
29. Prodan, E.; Radloff, C.; Halas, N. J.; Nordlander, P. A Hybridization Model for the Plasmon Response of Complex Nanostructures. *Science* **2003**, *302*, 419–422.
30. Doering, W. E.; Piotti, M. E.; Natan, M. J.; Freeman, R. G. SERS as a Foundation for Nanoscale, Optically Detected Biological Labels. *Adv. Mater.* **2007**, *19*, 3100–3108.
31. Kneipp, K.; Kneipp, H.; Kneipp, J. Surface-Enhanced Raman Scattering in Local Optical Fields of Silver and Gold Nanoaggregatess—From Single-Molecule Raman Spectroscopy to Ultrasensitive Probing in Live Cells. *Acc. Chem. Res.* **2006**, *39*, 443–450.
32. Anker, J. N.; Hall, W. P.; Lyandres, O.; Shah, N. C.; Zhao, J.; Duyne, R. P. V. Biosensing with Plasmonic Nanosensors. *Nat. Mater.* **2008**, *7*, 442–453.
33. Kneipp, N.; Kneipp, H.; Itzkan, I.; Dasari, R. R.; Feld, M. S. Ultrasensitive Chemical Analysis by Raman Spectroscopy. *Chem. Rev.* **1999**, *99*, 2957–2976.
34. Krug, J. T.; Wang, G. D.; Emory, S. R.; Nie, S. M. Efficient Raman Enhancement and Intermittent Light Emission Observed in Single Gold Nanocrystals. *J. Am. Chem. Soc.* **1999**, *121*, 9208–9214.
35. Fang, C.; Agarwal, A.; Buddharaju, K. D.; Khalid, N. M.; Salim, S. M.; Widjaja, E.; Garland, M. V.; Balasubramanian, N.; Kwong, D. L. DNA Detection Using Nanostructured SERS Substrates with Rhodamine B as Raman Label. *Biosens. Bioelectron.* **2008**, *24*, 216–221.
36. Qian, X. M.; Peng, X. H.; Ansari, D. O.; Goen, Q. Y.; Chen, G. Z.; Shin, D. M.; Yang, L.; Young, A. N.; Wang, M. D.; Nie, S. M. *In Vivo* Tumor Targeting and Spectroscopic Detection with Surface-Enhanced Raman Nanoparticle Tags. *Nat. Biotechnol.* **2008**, *26*, 83–90.
37. Tkachenko, A. G.; Xie, H.; Coleman, D.; Glomm, W.; Ryan, J.; Anderson, M. F.; Franzen, S.; Feldheim, D. L. Multifunctional Gold Nanoparticle−Peptide Complexes for Nuclear Targeting. *J. Am. Chem. Soc.* **2003**, *125*, 4700–4701.
38. Hirayama, K.; Akashi, S.; Furuya, M.; Fukuhara, K. L. Rapid Confirmation and Revision of the Primary Structure of Bovine Serum Albumin by ESIMS and Frit-FAB LC/MS. *Biochem. Biophys. Res. Commun.* **1990**, *173*, 639–646.
39. Xie, J.; Lee, J. Y.; Wang, D. I. C. Synthesis of Single-Crystalline Gold Nanoplates in Aqueous Solutions through Biomineralization by Serum Albumin Protein. *J. Phys. Chem. C* **2007**, *111*, 10226–10232.
40. Kneipp, J.; Kneipp, H.; McLaughlin, M.; Brown, D.; Kneipp, K. *In Vivo* Molecular Probing of Cellular Compartments with Gold Nanoparticles and Nanoaggregates. *Nano Lett.* **2006**, *6*, 2225–2231.
41. Gao, X. H.; Chan, W. C. W.; Nie, S. M. Quantum-Dot Nanocrystals for Ultrasensitive Biological Labeling and Multicolor Optical Encoding. *J. Biomed. Opt.* **2002**, *7*, 532–537.